Green Chemistry

Cutting-edge research for a greener sustainable future

www.rsc.org/greenchem

Volume 14 | Number 9 | September 2012 | Pages 2355–2648

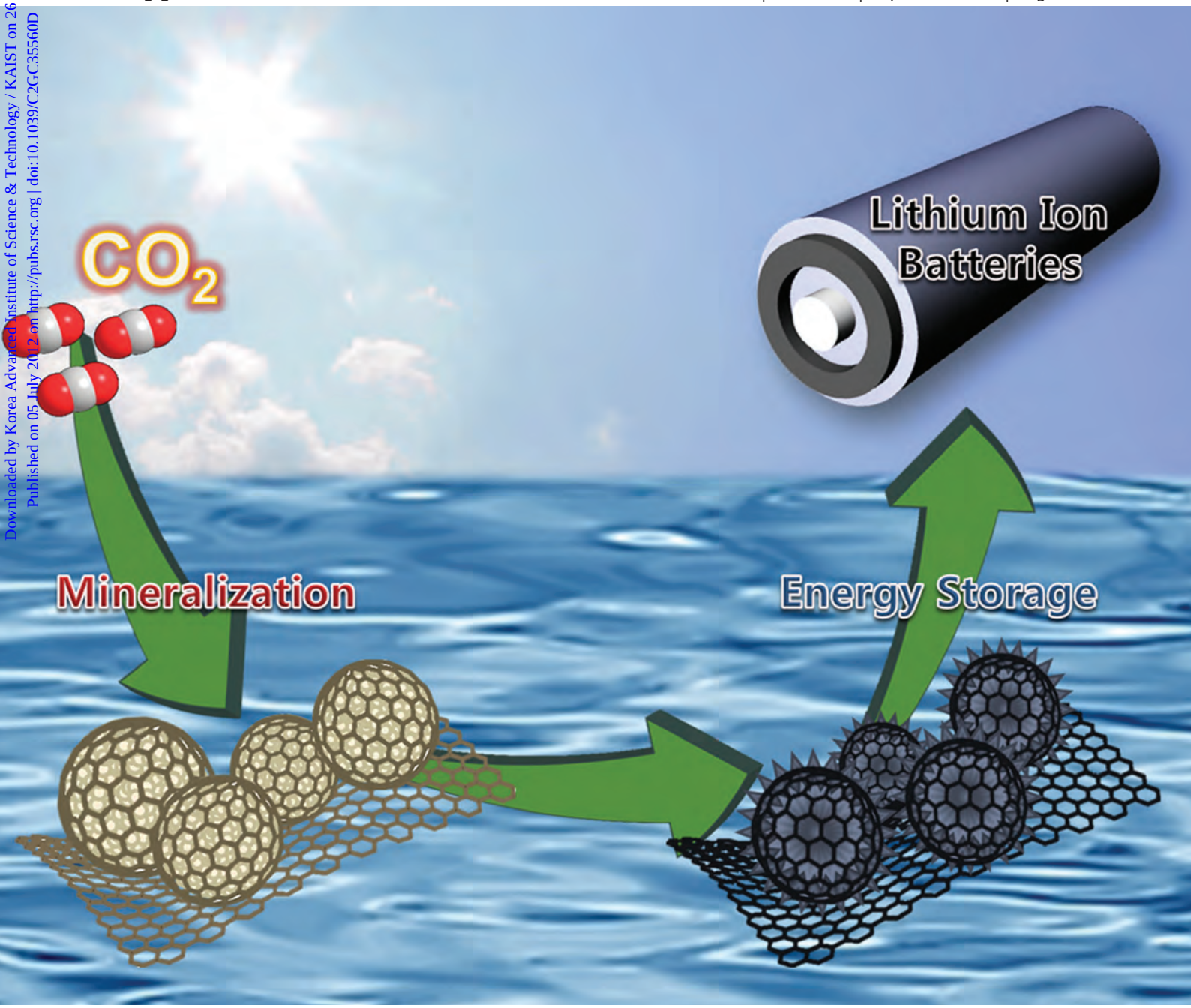

ISSN 1463-9262

RSC Publishing

COVER ARTICLE

Park *et al.*

Synthesis of graphene-wrapped CuO hybrid materials by CO_2 mineralization

Green Chemistry

Cite this: *Green Chem.*, 2012, **14**, 2391

www.rsc.org/greenchem

COMMUNICATION

Synthesis of graphene-wrapped CuO hybrid materials by CO_2 mineralization†

Jong Wan Ko,[a] Sung-Wook Kim,[b] Jihyun Hong,[b] Jungki Ryu,[a] Kisuk Kang[b] and Chan Beum Park*[a]

Received 14th April 2012, Accepted 3rd July 2012
DOI: 10.1039/c2gc35560d

Graphene-wrapped metal oxide hybrid materials are synthesized through inspiration from natural CO_2 mineralization. We created hierarchical, nanostructured graphene/metal oxide by converting a CO_2-mineralized graphene oxide/$CaCO_3$ precursor to metal-based minerals such as graphene-wrapped CuO hybrid materials, which highly enhanced the stability and recyclability of the CuO anode for Li ion batteries. The synthesis of graphene-wrapped metal oxide and its application to Li ion battery electrodes suggest a new possibility for hybridizing graphene and metal oxide nanoparticles using the inspiration of natural mineralization.

In nature, biological minerals exhibit fascinating morphologies with extraordinary physicochemical properties when hybridized with organic compounds.[1–6] In particular, biological systems store and utilize CO_2 gas in the form of organic–inorganic hybrid materials possessing vital biological functions. Aqueous creatures, such as mollusks and corals, use CO_2 dissolved in water as a primary source for the synthesis of bicarbonate-based biominerals.[1,4] For example, seashells synthesize strength-resistant exoskeletons made of complex and elaborate structures of $CaCO_3$ for protection and skeletal support. According to recent studies on *in vitro* biomineralization,[7–9] under mild conditions, hierarchical and sophisticated nanostructures of biominerals and their composites can be created through CO_2-storing biomineralization. For example, Kim *et al.*[9] synthesized hollow $CaCO_3$ microspheres and their composites with biodegradable polymer fibers by utilizing gaseous CO_2 in the presence of dopamine, a biomimetic molecule of adhesive foot protein secreted from mussels.

Inspired by the mineralization process in nature, we have synthesized novel graphene/CuO hybrid materials from $CaCO_3$ microspheres mineralized on graphene oxide (GO) nanosheets, and demonstrated that the hybrid composite is a promising electrode material for lithium ion batteries (LIBs). Among many systems for electrical energy storage, LIBs are widely used in mobile electronic equipment.[10] To meet the demands for increased LIB power and energy density, nanomaterials are drawing attention because they have a high specific surface area and enhance the transport of electrons and Li ions.[10,11] CuO is an abundant metal oxide that serves as electrode materials for LIBs, possessing high theoretical capacity and safety with low cost and limited environmental toxicity;[12,13] however, a large volumetric change of CuO electrodes during the insertion and extraction of Li ions can destroy its crystal structure and cause capacity decay in a short time.[14] According to the present work, graphene-wrapped CuO hybrid material that is synthesized *via* CO_2 mineralization can enhance the stability and recyclability of the CuO anode for LIBs. We have chosen graphene, a two-dimensional sp^2 carbon nanosheet, as a constituent of the hybrid material. Graphene is an attractive graphitic material because it exhibits high electrical mobility and conductivity as well as distinguished physical features like a large specific area and a high Young's modulus.[15–17]

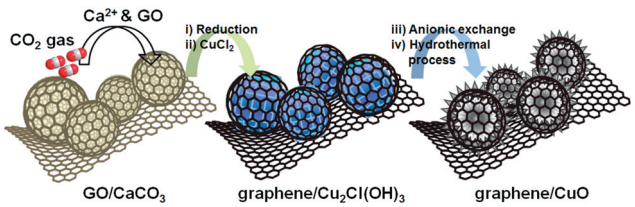

Fig. 1 Schematic illustration of sequential steps for the synthesis of graphene/CuO. GO/$CaCO_3$ was prepared by applying CO_2 gas to Ca^{2+} and GO suspension. Graphene/$Cu_2Cl(OH)_3$ was formed by chemical reduction of GO to graphene and transformation of $CaCO_3$ into $Cu_2Cl(OH)_3$. Graphene/CuO was synthesized from graphene/$Cu_2Cl(OH)_3$ by anionic exchange and a hydrothermal process.

Graphene-wrapped CuO (or graphene/CuO) hybrid material was synthesized according to the steps illustrated in Fig. 1. GO/$CaCO_3$ was prepared by applying CO_2 gas to a GO-suspended $CaCl_2$ solution. According to our previous work,[18,21] vaterite microspheres, the least stable of $CaCO_3$ polymorphs (*i.e.*, calcite, aragonite, and vaterite), are stabilized in the presence of graphene oxide and they could be transformed into bone minerals such as hydroxyapatite. We synthesized graphene/$Cu_2Cl(OH)_3$ by dispersing GO/$CaCO_3$ in hydrazine solution for the reduction of GO to graphene. We then transformed $CaCO_3$ into $Cu_2Cl(OH)_3$ in an acidic $CuCl_2$ solution (pH < 3). The $CaCO_3$ in graphene/$CaCO_3$ completely dissolved in Ca^{2+}

[a]*Department of Materials Science and Engineering, KAIST, Science Road 335, Yuseong-gu, Daejeon 305-701, Republic of Korea. E-mail: parkcb@kaist.ac.kr; Fax: +82 42 350 3310; Tel: +82 42 350 3340*
[b]*Department of Materials Science and Engineering, Seoul National University, Gwanak-ro, Gwanak-gu, Seoul 151-742, Republic of Korea*

†Electronic supplementary information (ESI) available: Experimental details and supporting data of SEM, TEM, XRD, and TGA. See DOI: 10.1039/c2gc35560d

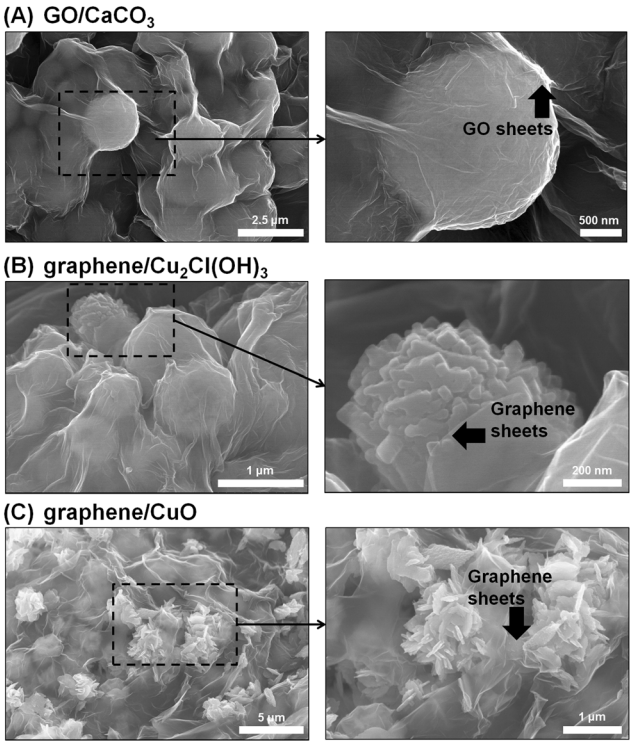

Fig. 2 (A) SEM images of $GO/CaCO_3$ showing $CaCO_3$ microspheres well-wrapped by GO sheets. (B) SEM images of graphene/$Cu_2Cl(OH)_3$ exhibiting similar morphology to $GO/CaCO_3$ with spherical inorganic particles, $Cu_2Cl(OH)_3$, integrated with graphene sheets. (C) SEM images of graphene/CuO showing CuO nanoribbons assembled into sea urchin-like microparticles hybridized with graphene.

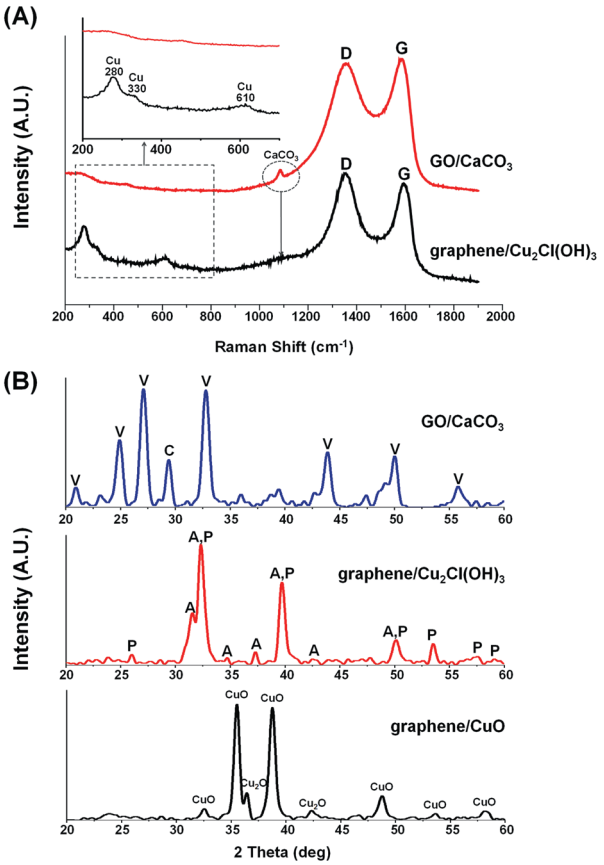

Fig. 3 (A) Raman shift spectra of $GO/CaCO_3$ and graphene/$Cu_2Cl(OH)_3$. The spectra show distinguished peaks at around 1350 and 1600 cm^{-1}, indicating disorder and vibration bands of graphite, respectively. The inset is a magnified image of the boxed region in the spectra. In the case of graphene/CuO, a Raman spectrum could not be obtained due to strong interference between graphene and CuO. (B) Powder XRD patterns of $GO/CaCO_3$, graphene/$Cu_2Cl(OH)_3$, and graphene/CuO. The patterns show sequential substitution of inorganic components during synthesis steps. V and C indicate vaterite and calcite phases of $CaCO_3$, respectively.

and CO_3^{2-} ions in the acidic $CuCl_2$ solution, and the nucleation of Cu-containing inorganic minerals was initiated according to the following reaction: $CaCO_3(s) + 2CuCl_2(aq) + 2H_2O \rightarrow Cu_2Cl(OH)_3(s) + HCl(aq) + CaCl_2(aq) + CO_2(g)$.[19] We further substituted Cl^- ions with OH^- ions in the graphene/$Cu_2Cl(OH)_3$ by incubating them in NaOH solution to prepare graphene/$Cu(OH)_2$. Finally, we removed H_2O from graphene/$Cu(OH)_2$ through a hydrothermal reaction in order to create graphene/CuO hybrid material.

Morphological characteristics of $GO/CaCO_3$, graphene/$Cu_2Cl(OH)_3$, and graphene/CuO were observed by using a scanning electron microscope (SEM). Fig. 2A and Fig. S1A† show SEM images of $GO/CaCO_3$ prepared by CO_2 mineralization in the presence of GO. The images indicate that each $CaCO_3$ microsphere is well wrapped by GO sheets. The SEM images of graphene/$Cu_2Cl(OH)_3$ in Fig. 2B and Fig. S1B† show that graphene sheets fully cover 'rocky-shaped' $Cu_2Cl(OH)_3$ microparticles, indicating the conversion of $CaCO_3$ to $Cu_2Cl(OH)_3$ while retaining the morphology of two-dimensional carbon sheets covering inorganic particles. According to Raman spectroscopic analysis (Fig. 3A), the peak corresponding to $CaCO_3$ at 1100 cm^{-1} disappeared. Meanwhile, the corresponding peaks for the Cu element showed up in graphene/$Cu_2Cl(OH)_3$ at the wave numbers of 280, 330, and 610 cm^{-1}. In comparison with $GO/CaCO_3$, the Raman spectrum of graphene/$Cu_2Cl(OH)_3$ indicates that D and G peaks shifted from 1363 and 1594 cm^{-1} to 1352 and 1584 cm^{-1}, respectively, with an increased D/G peak ratio. The increased ratio of D/G intensity was interpreted to indicate the successful reduction of GO to graphene.[20] The SEM images of graphene/CuO in Fig. 2C and Fig. S1C† show that nanoribbon-like CuO aggregates are well-hybridized with graphene sheets. We further compared the morphologies of $GO/CaCO_3$ and graphene/CuO by using a transmission electron microscope (Fig. S2†). The surface of the $CaCO_3$ microsphere was wrapped by GO sheets (Fig. S2A and S2B†); similarly, nanostructured CuO aggregates were firmly covered by graphene sheets (Fig. S2C and S2D†). When we synthesized CuO by CO_2 mineralization in the absence of graphene oxide, a rhombohedral calcite phase of $CaCO_3$ was formed, and the calcite $CaCO_3$ was converted to $Cu_2Cl(OH)_3$ and CuO that exhibited significantly different size and structure compared to CuO nanoribbons in the graphene hybrid materials (Fig. S3†).

We examined crystal structure changes of each hybrid material by using an X-ray diffractometer (XRD) (Fig. 3B). According to the XRD pattern of $GO/CaCO_3$, $CaCO_3$ in the composite exists mainly in the vaterite phase with a relatively small amount in the

calcite phase. Vaterite, the least stable phase of $CaCO_3$, is stabilized because of functional groups in GO, such as epoxy, hydroxyl, and carboxyl groups. These groups inhibit the phase transformation of vaterite to the thermodynamically more stable calcite phase.[21] Among copper chloride hydroxide polymorphs with $Cu_2Cl(OH)_3$ stoichiometry, the XRD pattern of graphene/$Cu_2Cl(OH)_3$ was indexed as orthorhombic atacamite (JCPDS card No. 25-0269) and rhombohedral paratacamite (JCPDS card No. 50-1560). In nature, atacamite is a Cu-based biomineral that exhibits high mechanical strength.[1] In the XRD pattern of graphene/CuO, we observed typical diffraction peaks of CuO having a monoclinic structure (space group $C2/c$, a = 4.686 Å, b = 3.425 Å, c = 5.129 Å, β = 99.47°, JCPDS card No. 05-0661) with relatively smaller peaks of Cu_2O.

X-ray photoelectron spectroscopy (XPS) analysis was further conducted to compare chemical compositions of GO/$CaCO_3$ and graphene/CuO. The C 1s XPS spectrum of GO/$CaCO_3$ in Fig. S4A† shows multiple peaks at 284.6, 286.7, 288.0, and 289.1 eV. These peaks correspond to graphite, epoxy, C═O, and C(O)O groups in GO, respectively. Two additional peaks at 285.0 eV of hydrocarbon and 289.3 eV of carbonate from $CaCO_3$ were observed in GO/$CaCO_3$. Fig. S4B† exhibits two distinguished peaks of Ca $2p_{3/2}$ and Ca $2p_{1/2}$ at 347.3 and 350.9 eV, respectively.

In Fig. S4C,† the increased ratio of the graphite/epoxy peak compared to that in Fig. S4A† confirms the presence of graphene in graphene/CuO hybrid materials. The binding energy peak of C–N originating from hydrazine treatment also appears at 285.6 eV. The XPS spectrum of Cu 2p in Fig. S4D† confirms that CuO exists as a major phase in the hybrid material between two copper oxide forms. The main peak of Cu $2p_{3/2}$ appears at 933.9 eV and an additional peak of Cu $2p_{1/2}$ shows up at 953.7 eV. The main peak represents Cu^{2+} ions on the surface of graphene/CuO, rather than Cu^{+} ions (having a main peak of Cu 2p at 932.4 eV).[22] According to the literature,[13,23] this peak can be ascribed to the configuration of a partially-filled d-shell, suggesting that only 9 electrons exist as d^9 configurations at the ground state of Cu atoms in the hybrid material. Wide-range XPS scans ranging from 0 to 1300 eV in Fig. S5† show multiple peaks corresponding to Cu with C and O elements for the graphene/CuO hybrid and C, Ca, and O elements for GO/$CaCO_3$. According to a recent report,[24] an incipient wetness impregnation of $CuCl_2$ and graphene produces urchin-like CuO-decorated graphene composites but in a broad distribution of particle size. The method requires the use of organic solvent (*e.g.*, isopropyl alcohol) under elevated temperature and basic pH. In contrast, our process can synthesize more uniform CuO nanoribbons (100–300 nm) that are wrapped by graphene sheets while using environmentally-friendly conditions: use of CO_2 gas and biominerals ($CaCO_3$, atacamite) in an aqueous solution. It is noteworthy that the intermediate material in the two-step process includes $Cu_2Cl(OH)_3$, which is a Cu-based natural biomineral (*i.e.*, atacamite) found in the jaws of marine bloodworm *Glycera dibranchiate*.[1]

To examine the potential of graphene/CuO as an energy storage material, we performed electrochemical tests of the hybrid material on an LIB system. In an LIB system, facile Li-ion and electron transport is essential for the electrochemical reaction to convert electric energy to chemical energy. CuO is known to possess high energy storage capability through a conversion reaction.[25] The theoretical capacity of CuO (673 mAh g^{-1}) is approximately 1.8 times higher than that of the conventional graphite anode (372 mAh g^{-1}). The nanoscopic nature of CuO in the hybrid material was expected to enhance Li-ion transport due to large surface area and short Li-ion penetration distance, thus resulting in improved electrochemical activity. In graphene/CuO hybrid materials, individual CuO nanoribbons are attached to the highly conductive graphene surface; hence, electrons could be supplied easily during the electrochemical reaction. In addition, graphene itself is a good energy storage material for LIB. Yoo *et al*. recently reported that the graphene nanosheet exhibits better Li-ion storage capability than graphite.[26] In this respect, graphene in the hybrid material not only provides an efficient pathway for electron transport, but also stores Li-ions to enhance LIB performance. To determine the content of graphene in the hybrid material, we conducted thermal gravimetric analysis from room temperature to 800 °C under air (Fig. S6†). The weight loss was observed to be 13.5% at around 420 °C, due to the combustion of carbon–carbon linkage in graphene sheets.[27,28] This graphene content is considered to be sufficient to influence battery performance.

Electrochemical properties of graphene/CuO in comparison with that of commercially available CuO nanoparticles (nano-CuO, size < 50 nm) were investigated using cyclic voltammetry (CV). The morphology and XRD pattern of nano-CuO are shown in Fig. S9.† Fig. S7† displays CV curves of nano-CuO and graphene/CuO hybrid materials at a scan rate of 0.1 mV s^{-1}. Three cathodic peaks were observed at 1.92, 1.13, and 0.81 V (*vs*. Li/Li^+) in the first discharge cycle of graphene/CuO, which correspond to the conversion of (1) CuO to Cu_2O, (2) Cu_2O to Cu, and (3) the formation of Li_2O (overall reaction: CuO + 2Li ↔ Cu^0 + Li_2O), respectively.[25] During the charging step, anodic peaks located at 1.29, 2.42, and 2.71 V were recorded by reversible reactions. In the case of nano-CuO, cathodic peaks at 1.62, 1.08, and 0.77 V and anodic peaks at 0.79 and 2.46 V were observed in the first cycle, which were different from those of graphene/CuO. In the second cycle, decreases of individual cathodic peak intensities and integrated areas were observed along with shifts of the peaks in both CV curves. In particular, a more drastic change in peak intensities and integrated areas was observed for nano-CuO when compared to graphene/CuO in the second cycle, which indicates higher irreversible capacity of nano-CuO. We attribute the differential result to the presence of conductive graphene in the hybrid materials that should facilitate the shuttling of Li^+ ions between CuO and electrolyte interfaces.

Battery performance of graphene/CuO and nano-CuO is shown in Fig. 4. At the first discharge at a current rate of 100 mA g^{-1}, both graphene/CuO and nano-CuO exhibited exceptionally high specific capacity compared to the theoretical capacity (Fig. 4A). This finding is attributed to the high surface area of both materials, which can induce irreversible side reactions with electrolytes.[11,29] After the first discharge at the same current rate, the specific capacity of graphene/CuO was saturated to approximately 600 mAh g^{-1}, which is comparable to the theoretical capacity (673 mAh g^{-1}). In contrast, nano-CuO showed poor electrochemical activity (<300 mAh g^{-1}) and the

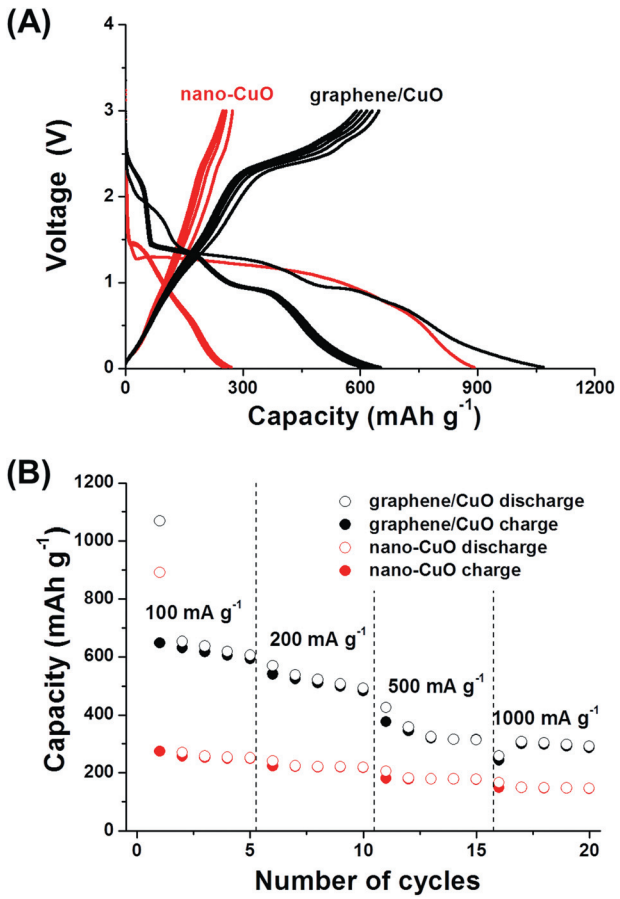

Fig. 4 (A) Charge/discharge profiles of graphene/CuO and commercial nano-CuO at a current density of 100 mA g^{-1}. (B) Specific capacity of graphene/CuO and nano-CuO at different current densities from 100 to 1000 mA g^{-1}.

cell voltage of nano-CuO drastically changed according to capacity. The specific surface area of graphene/CuO (33.61 m^2 g^{-1}) was slightly larger than that of nano-CuO (29.22 m^2 g^{-1}). But graphene/CuO and nano-CuO possessed significantly different electrochemical profiles, as shown in Fig. 4A. In the case of graphene/CuO, a sufficient supply of electrons can occur through the layer of graphene, while the strong attachment of CuO to graphene reduces the strain, resulting in improved electrochemical performances. In addition, graphene/CuO showed much higher capacity, which was well retained at the prolonged cycles, when compared to those of nano-CuO (Fig. S8†).

In summary, hierarchical nanostructured graphene/CuO hybrid materials can be successfully synthesized by converting a CO_2-mineralized GO/$CaCO_3$ precursor to Cu-based minerals. Graphene/CuO exhibited nanoribbon-like CuO aggregates well-hybridized with graphene nanosheets. The graphene-wrapped CuO showed high potential as an LIB anodic material compared to commercial nano-CuO particles. The excellent electrochemical performance of graphene/CuO is attributed to the synergic effect of (1) CuO wrapped by highly conductive graphene sheets and (2) graphene itself capable of Li-ion storage. Furthermore, flexible graphene sheets hybridized with CuO were beneficial for reducing the strain caused by volume changes during the charge/discharge process to show good cyclic performance. The synthesis of graphene/CuO and its application to LIB electrodes suggest a new possibility for hybridizing graphene and metal oxide nanoparticles using the inspiration of natural mineralization.

Acknowledgements

This study was supported by the National Research Foundation (NRF) *via* the National Research Laboratory (R0A-2008-000-20041-0), Converging Research Center (2009-0082276), and Intelligent Synthetic Biology Center of Global Frontier Project (2011-0031957).

Notes and references

1 A. Sigel, H. Sigel and R. K. O. Sigel, Metal Ions in Life Sciences Vol. 4 Biomineralization, *From Nature to Application*, John Wiley & Sons Ltd, Chichester, UK, 2008.
2 A. Sellinger, P. M. Weiss, A. Nguyen, Y. Lu, R. A. Assink, W. Gong and C. J. Brinker, *Nature*, 1998, **394**, 256.
3 L. Addadi, S. Raz and S. Weiner, *Adv. Mater.*, 2003, **15**, 959.
4 S. Mann, *Biomineralization: Principles and Concepts in Bioinorganic Materials Chemistry*, Oxford University Press, Oxford, UK, 2001.
5 I. A. Aksay, M. Trau, S. Manne, I. Honma, N. Yao, L. Zhou, P. Fenter, P. M. Eisenberger and S. M. Gruner, *Science*, 1996, **273**, 892.
6 Z. Tang, N. A. Kotov, S. Magonov and B. Ozturk, *Nat. Mater.*, 2003, **2**, 413.
7 C.-L. Chen, J. Qi, R. N. Zukermann and J. J. DeYoreo, *J. Am. Chem. Soc.*, 2011, **133**, 5214.
8 J. Xiao and S. Yang, *Adv. Eng. Mater.*, 2011, **13**, B32.
9 S. Kim, J. W. Ko and C. B. Park, *J. Mater. Chem.*, 2011, **21**, 11070.
10 P. G. Bruce, B. Scrosati and J.-M. Tarascon, *Angew. Chem., Int. Ed.*, 2008, **47**, 2930.
11 Z.-S. Wu, W. Ren, L. Wen, L. Gao, J. Zhao, Z. Chen, G. Zhou, F. Li and H.-M. Cheng, *ACS Nano*, 2010, **4**, 3187.
12 N. Li, Z. Wang, K. Zhao, Z. Shi, S. Xu and Z. Gu, *J. Nanosci. Nanotechnol.*, 2010, **10**, 6690.
13 J. Zhu, G. Zeng, F. Nie, X. Xu, S. Chen, Q. Han and X. Wang, *Nanoscale*, 2010, **2**, 988.
14 L. B. Chen, N. Lu, C. M. Xu, H. C. Yu and T. H. Wang, *Electrochim. Acta*, 2009, **54**, 4198.
15 S. Chen, J. Zhu, X. Wu, Q. Han and X. Wang, *ACS Nano*, 2010, **4**, 2822.
16 Y. Xu, H. Bai, G. Lu, C. Li and G. Shi, *J. Am. Chem. Soc.*, 2008, **130**, 5856.
17 Y. Zhu, S. Murali, W. Cai, X. Li, J. W. Suk, J. R. Potts and R. S. Ruoff, *Adv. Mater.*, 2010, **22**, 3906.
18 S. Kim and C. B. Park, *Biomaterials*, 2010, **31**, 6628.
19 Y. Ma, C. Lin, Y. Jiang, W. Lu, C. Si and Y. Liu, *J. Hazard. Mater.*, 2009, **172**, 1288.
20 S. Stankovich, D. A. Dikin, R. D. Piner, K. A. Kohlhaas, A. Kleinhammes, Y. Jia, Y. Wu, S. T. Nguyen and R. S. Ruoff, *Carbon*, 2007, **45**, 1558.
21 S. Kim, S. H. Ku, S. Y. Lim, J. H. Kim and C. B. Park, *Adv. Mater.*, 2011, **23**, 2009.
22 Z. H. Gan, G. Q. Yu, B. K. Tay, C. M. Tan, Z. W. Zhao and Y. Q. Fu, *J. Phys. D: Appl. Phys.*, 2004, **37**, 81.
23 M. Ni and B. D. Ratner, *Surf. Interface Anal.*, 2008, **40**, 1356.
24 L. Qiang and Y. Wang, *Electrochem. Commun.*, 2012, **14**, 82.
25 X. P. Gao, J. L. Bao, G. L. Pan, H. Y. Zhu, P. X. Huang, F. Wu and D. Y. Song, *J. Phys. Chem. B*, 2004, **108**, 5547.
26 E. J. Yoo, J. Kim, E. Hosono, H.-S. Zhou, T. Kudo and I. Honma, *Nano Lett.*, 2008, **8**, 2277.
27 S. Park, J. An, I. Jung, R. D. Piner, S. J. An, X. Li, A. Velamakanni and R. S. Ruoff, *Nano Lett.*, 2009, **9**, 1593.
28 H. Chen, M. B. Muller, K. J. Gilmore, G. G. Wallace and D. Li, *Adv. Mater.*, 2008, **20**, 3557.
29 S. Yang, G. Cui, S. Ping, Q. Cao, U. Kolb, X. Feng, J. Maier and K. Mullen, *ChemSusChem*, 2010, **3**, 236.

